Review

Near-infrared mechanoluminescence crystals: a review

Puxian Xiong,[1] Mingying Peng,[1,2,*] and Zhongmin Yang[1,2,*]

SUMMARY

Due to the *in situ*, real-time, and non-destructive properties, mechanolumines-cence (ML) crystals have been considered as intelligent stress sensors, which demonstrate potential applications such as in inner crack visualization, light source, and ultrasonic powder recording. Thereinto, it is highly expected that near-infrared (NIR) MLs can realize the visualization of inner biological stress because mechanically induced signals from them can penetrate biological tissues. However, such an energy conversion technique fails to work in biomechanical monitoring due to the limited advances of NIR ML materials. Based on those, some research groups have begun to focus on this field and initially realized this idea *in vitro* while related advances are still at the early stage. To advance this field, it is highly desirable to review recent advances in NIR ML crystals. In this review, to our knowledge, all the NIR ML crystals have been included in two main groups: oxysulfides and oxides. Besides, the present and emerging trends in investigation of such crystals were discussed. In all, the aim is to advance NIR ML crystals to more practical applications, especially for that of biomechanical visualization *in vivo*.

INTRODUCTION

Mechanoluminescence (ML) is an amazing physical phenomenon of a material (usually a solid), which emits corresponding to external mechanical stimuli such as friction, impact, compression, and bending (Wang et al., 2019; Zhang et al., 2019). It exists in both inorganic and organic compounds (Feng and Smet, 2018; Xie and Li, 2018). Generally, it is recognized that Francis Bacon made the first documented ML in 1605: "sugar shineth only while in scraping" (Bacon, 1863), which is now classified as fractoluminescence accompanied by the structure destruction of the material leading to limited applications. In 1999, Xu et al. developed two classic elastic ML materials (ZnS:Mn^{2+} and SrAl$_2$O$_4$:Eu^{2+} [only monoclinic phase SrAl$_2$O$_4$]) whose ML intensities can be fully restored keeping complete crystal structure (Xu et al., 1999a, 1999b). From then on, the development of ML has advanced a big step during the past two decades (Figure 1) (Notably, the word "ML" in this review only consists of elastic ML materials.). Thereinto, visible ML based on various hosts was reported such as in aluminates (Akiyama et al., 1998; Xu et al., 2000), gallates (Matsui et al., 2000), titanates (Wang et al., 2005), silicates (Zhang et al., 2010), and stannates (Kamimura et al., 2012). Typically, the nature of visible ML optical centers can be lanthanide (Eu^{2+}, Sm^{3+}, Pr^{3+}, etc) or transition metal (Cu$^+$ and Mn^{2+}) ion. Besides, visible ML has covered the whole visible spectral range (380–760 nm). Based on those, ML materials have found huge potential applications such as in crack visualization (Kundu et al., 2012), photo-catalysis (Terasaki et al., 2013), smart display (Jeong et al., 2014), energy storage and conversion (Zhuang et al., 2020), and photonic skin (Qian et al., 2018). While as for the applications in bioimaging, to our knowledge, limited progress has been made.

Remarkably, as a novel non-destructive, *in situ*, real-time, and non-contact mechano-opto-responsive technique, ML is highly expected to find practical applications in bioimaging to help study the complex biomechanical behaviors of our body or corresponding artificial implants. Compared to traditional bioimaging ones, the demands in biological imaging urge such ML materials to possess stronger intensities, shorter response times, and lower costs with flexible wavelengths (Huang et al., 2017a). Indeed, researchers have tried to develop such biocompatible ML-based materials and devices, while few researchers have focused on the *in vivo* biomechanical detection (Larson et al., 2016; Tan et al., 2020). Thereinto, the difficulty in non-contact exciting ML probes from outside of the body should be one reason. However, if one has been aware that acoustic shock or pulsed infrared laser (both can penetrate tissues) also can induce ML,

[1]School of Physics and Optoelectronic, State Key Laboratory of Luminescent Materials and Devices, Guangdong Provincial Key Laboratory of Fiber Laser Materials and Applied Techniques, South China University of Technology, Guangzhou 510640, China

[2]The China-Germany Research Center for Photonic Materials and Device, The State Key Laboratory of Luminescent Materials and Devices, Guangdong Provincial Key Laboratory of Fiber Laser Materials and Applied Techniques, The School of Materials Science and Engineering, South China University of Technology, Guangzhou 510641, China

*Correspondence:
pengmingying@scut.edu.cn (M.P.),
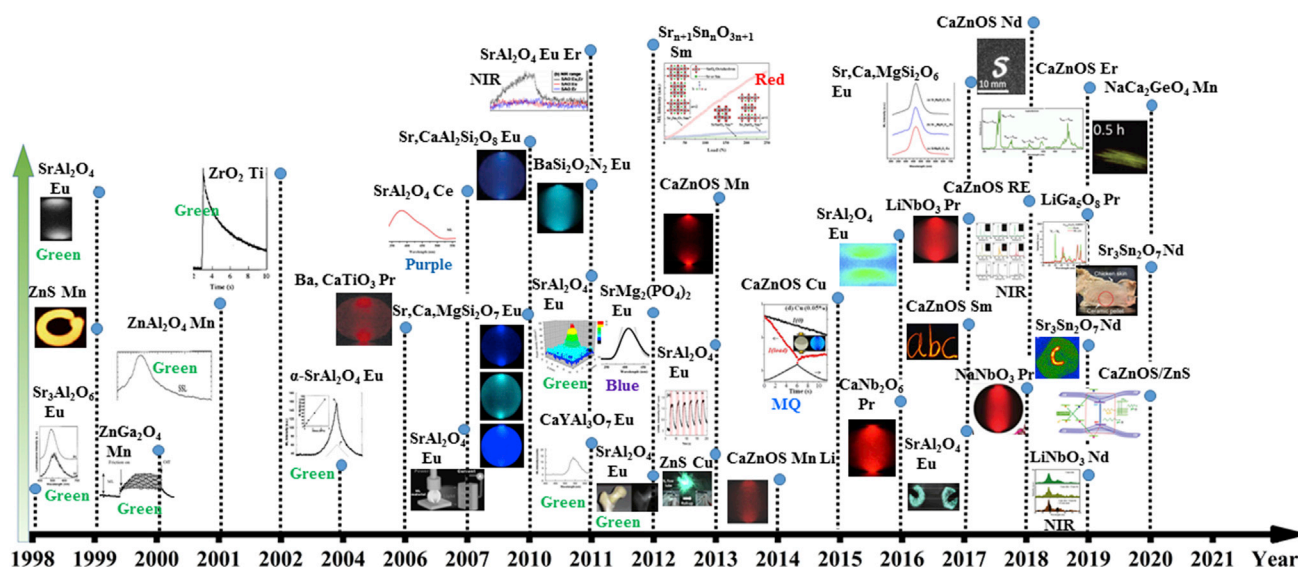yangzm@scut.edu.cn (Z.Y.)

Figure 1. Recent advances in the development of ML materials (year: 1998–2021)

this restriction may not exist (Eddingsaas and Suslick, 2006; Hardy et al., 1979). Also, very recently, Wu et al. used the brain-penetrant focused ultrasound to excite the local nano ML light sources (ZnS:Ag$^+$, Co^{2+}), such a method may provide a new idea to non-contact ML excitation mode in bioimaging (Wu et al., 2019). After solving the difficulty in ML exciting modes, detecting ML signals of biomechanical behaviors becomes the main problem. To avoid invasive delivery of detection equipment demonstrated such as by Zhang et al. (Zhang et al., 2020b), such ML signals are required to penetrate tissues (namely, near-infrared [NIR] MLs located within the tissue penetration biowindows), especially for implants such as an artificial bone which is deeply covered by other soft tissues. Although dual-energy X-ray absorptiometry or sonography can be used to assess the biomechanical quality of bones, they are expensive and require bulky devices (Liu and Webster, 2016). Other biomechanical sensors were developed to study the bone strength; however, they either require complex external equipment or they are not sensitive enough to enable in situ and real-time detection (Afsarimanesh et al., 2018). Hence, developing efficient NIR ML materials which can penetrate tissues for potential inner biomechanical visualization is urgently required. So, how is the development of NIR ML crystals? Disappointingly, even dating back to 1605, no more than 11 documented NIR ML crystals have been reported (Table 1). Obviously, the number of visible ML crystals far exceeds that of NIR. It is until the last 3 years that researchers began to show more interest in NIR MLs. The reasons behind this are as follows: First, one may easily mention that this may be because of the difference in common spectral detectors between visible (Si-CCD [charge-coupled device]) and NIR (usually InGaAs-CCD) band, which makes it "harder" to obtain NIR ML signals (Huang et al., 2017b). Second, no convincing NIR ML mechanisms have been established. Without theoretical guidance, all material exploration will only be trial and error, which has costed too much effort. Third, it is precisely because there is no direct application requirement related to NIR ML that the research development of this field is so slow.

In this review, to our knowledge, recent advances of all the existed NIR ML crystals are collected and are divided into two categories: oxysulfides and oxides (Notably, only ML based on inorganic crystals was discussed in this mini review. For non-crystalline MLs such as in organic systems, one can refer to corresponding review for details [Xie and Li, 2018]. Pure organic MLs have already found applications in health care [Wang et al., 2020], piezo-display [Li et al., 2018c], or impact sensor [Incel et al., 2017].). For known ML systems, only lanthanide ions (Nd^{3+}, Pr^{3+}, Yb^{3+}, Tm^{3+}, and so on) were confirmed to function as NIR ML emitters, where Nd^{3+} ion dominates the number in those NIR ML materials. Besides, data concerning crystal system, space group, and the exact chemical environment around NIR ML emitters such as coordination number (CN) and ion radii of the to-be-substituted host cation ions were also carefully discussed. Finally, series of challenges and outlooks were provided, which are highly expected to advance the development of NIR ML crystals. It is hoped that this review could shed light on the exploration of efficient NIR ML biomechanical detection probe materials.

Table 1. Known NIR ML crystals (collected whose MLs have been extended into the NIR range (780–1700 nm); year: 1605–2020)

Category		Host	Crystal system space group	Sites (CN, radii (Å))	Emitter	Bio-penetration tissues	Published year	Reference
I	Oxysulfides	CaZnOS	Hexagonal $P6_3mc$	Ca^{2+} (6, 1.000)	Nd^{3+}	Pork slices	Apr. 2018	(Li et al., 2018b)
		CaZnOS	Hexagonal $P6_3mc$	Ca^{2+} (6, 1.000)	Pr^{3+}, etc	/	Dec. 2018	(Du et al., 2018)
		$SrZn_2S_2O$	Orthorhombic $Pmn2_1$	Sr^{2+} (6, 1.180)	Yb^{3+}	/	Nov. 2019	(Chen et al., 2020)
		SrZnSO	Hexagonal $P6_3mc$	Sr^{2+} (6, 1.180)	Nd^{3+}, etc	/	Nov. 2019	(Chen et al., 2020)
		CaZnOS	Hexagonal $P6_3mc$	Ca^{2+} (6, 1.000)	Er^{3+}, etc.	/	Dec. 2019	(Li et al., 2020)
II	Aluminates	$SrAl_2O_4$	Monoclinic $P2_1$	Sr^{2+} (6, 1.180)	Er^{3+}	/	/, 2011	(Terasawa et al., 2011)
		$SrAl_2O_4$	Monoclinic $P2_1$	Sr^{2+} (6, 1.180)	Nd^{3+}	/	Sep. 2020	(Fujio et al., 2020)
	Gallates	$LiGa_5O_8$	Cubic $P4_332$	Li^+ (6, 0.760)	Pr^{3+}	Pork	Sep. 2019	(Xiong et al., 2019b)
	Niobates	$LiNbO_3$	Trigonal $R3c$	Li^+ (6, 0.760)	Nd^{3+}	Pork	Apr. 2019	(Xiong and Peng, 2019)
	Stannates	$Sr_3Sn_2O_7$	Orthorhombic $Cmcm$	Sr^{3+} (9, 1.310)	Nd^{3+}	Pork, HAP	Mar. 2019	(Xiong et al., 2019a)
		$Sr_3Sn_2O_7$	Orthorhombic $A2_1am$	Sr^{3+} (9, 1.310)	Nd^{3+}	Pork, chicken	May 2020	(Tu et al., 2020)

KNOWN NIR MECHANOLUMINESCENT CRYSTALS

Oxysulfides

CaZnOS

Generally, to design an NIR ML material, two aspects should be considered. One is to confirm a suitable host for a dopant with desired NIR emission and another is to regulate related luminescence quenching and energy-level mismatch, which determine whether NIR ML will appear. Based on the known fact that CaZnOS can accommodate for most rare-earth (RE) ions to have visible MLs, in 2018, Li et al. reported that Nd^{3+} ion-doped CaZnOS could emit under external force (compression/friction) (Figure 2) (Li et al., 2018b). ML signals span from the first (650–950) to the second (950–1400) NIR tissue-penetrating bio-imaging window. For this regard, when the force reaches up to 5 kN, the NIR ML emission can penetrate tissues (pork) as deep as 22 mm. Besides, NIR ML signals from the sample bitten by human teeth with mouth open or closed were also observed, demonstrating that such NIR MLs can be generated by biomechanically teeth biting and have good tissue penetration ability. Moreover, such force-response behavior is highly reproducible after proper recharging by UV irradiation. This work has expanded the potential applications of ML into biomedical fields. This should be attributed to such high ML sensitivity of CaZnOS (d_{33} = 38 pm/V). This is reasonable from a certain point of view, and CaZnOS has indeed been proven to be one of the most classic ML hosts after ZnS with many published works within the visible range (Tu et al., 2014, 2015; Wang et al., 2017; Zhang et al., 2013, 2015). Except for this, another impactful work was also reported based on CaZnOS in 2018, which realized multicolor luminescence from visible to NIR range (~270–1000 nm, Figure 3) (Du et al., 2018). In this work, Du et al. proposed a lithium-assisted ($LiNO_3$) annealing method for effectively incorporating nearly all the RE ions into CaZnOS. Notably, this method is of great significance for improving the ML intensity because it has helped realize the NIR ML signals of Pr^{3+}, Ho^{3+}, and Dy^{3+} (in CaZnOS), and these NIR MLs were originally ignored. However, although many NIR MLs had been focused on in this compound, no related application demonstrations to NIR ML had been provided in this work. Afterward in 2019, Li et al. extended the NIR ML to ~1540 nm (Er^{3+} ions) at the third tissue biowindow (Li et al., 2020). Here, multiple NIR ML spectral bands from Er^{3+} such as 845–880 nm, 960–1000 nm, and 1450–1700 nm were demonstrated. At the material synthesis stage, Li_2CO_3 was added to regulate its ML performances (namely, CaZnOS:Er^{3+}, Li^+ is better than CaZnOS:Er^{3+} in both NIR ML sensitivity and intensity). Piezoresponse force microscopy was used to firstly confirm that both samples have good piezoelectric performances, and Li^+ codoping led to a higher piezoelectric coefficient, whose behind reason is attributed to the preferred crystal orientation after the addition of Li_2CO_3. Worth noting, *in situ* high-pressure study was also introduced to study inorganic ML powders, which aims to *in situ* probe both the luminescence properties and band structure. Finally, observations tend to indicate that the oriented migration of electrons which can be modulated or accelerated in a strain-induced piezoelectric field matters in the ML process. Compared with other NIR MLs, the "shortest" NIR ML wavelength (Er^{3+}: ~1540 nm) located within the so-called third biowindow (1500–1800 nm) was obtained. One should note that the Rayleigh
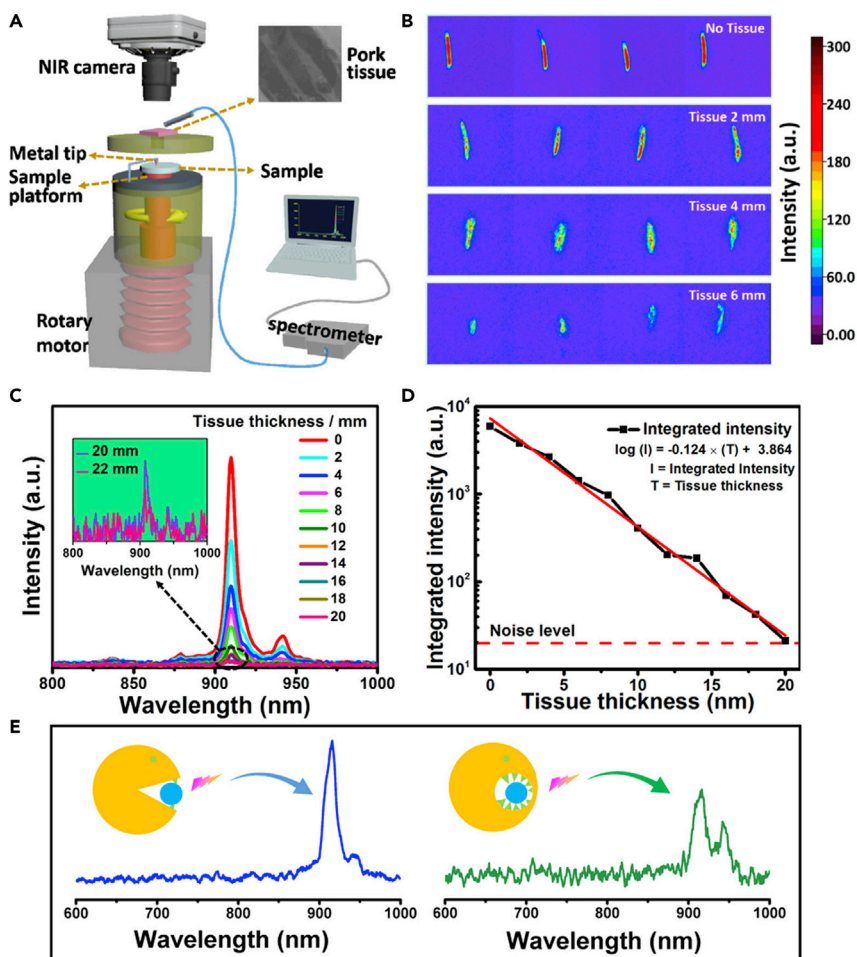
Figure 2. Demonstration of bioimaging with CaZnOS:1% Nd^{3+}

(A) The schematic diagram for imaging and spectroscopic detection of the NIR EML after passing through the tissue.

(B) Bioimaging of tissues by detecting NIR EML light passing through the tissues with different thicknesses.

(C) Emission spectra of NIR EML passing through the tissues with different thicknesses. Inset: emission spectra corresponding to tissue thickness of 20 and 22 mm.

(D) Tissue thickness-dependent log of integrated transmitted emission intensity. Red dash line shows the noise level, whereas red solid line shows the fitted results using a linear equation, $\log(I) = -0.124T + 3.864$, where I and T denote the integrated intensity and tissue thickness, respectively.

(E) NIR ML signal from the sample bitten by human teeth with mouth open (left) or mouth closed (right), showing that the NIR ML signal can be generated due to teeth biting and still be detected with closed mouth due to good tissue penetration capability. Reproduced with permission from (Li et al., 2018b). Copyright 2018 American Chemical Society.

scattering (varies as λ^{-4}, where λ is wavelength) will decrease as wavelength increases (Clays and Persoons, 1991); hence, NIR ML of Er^{3+} should give the lowest scattering coefficient to ensure an improved resolution quality and deeper penetration depth. However, authors may just have ignored such possible applications since we find no such demonstrations here.

Witnessing the development, researchers deeply realize that the applications of (NIR) ML are mostly limited by the weak and non-recoverable ML emissions. For this regard, numerous efforts have been paid to enhance the ML intensity such as by addition of fluxing agent (Zhang et al., 2020a), design of array structures (Bao et al., 2019), textile-assisted emission (Park et al., 2019), and regulation of reaction conditions (Wu et al., 2018). However, till now, quite limited MLs can be self-recoverable (no need of pre-irradiation to generate ML). For the self-recovery of ML, doped ZnS seems to have always stood out, which was attributed to the trapping of drifting charge carriers in the presence of piezoelectric field (Chandra et al.,
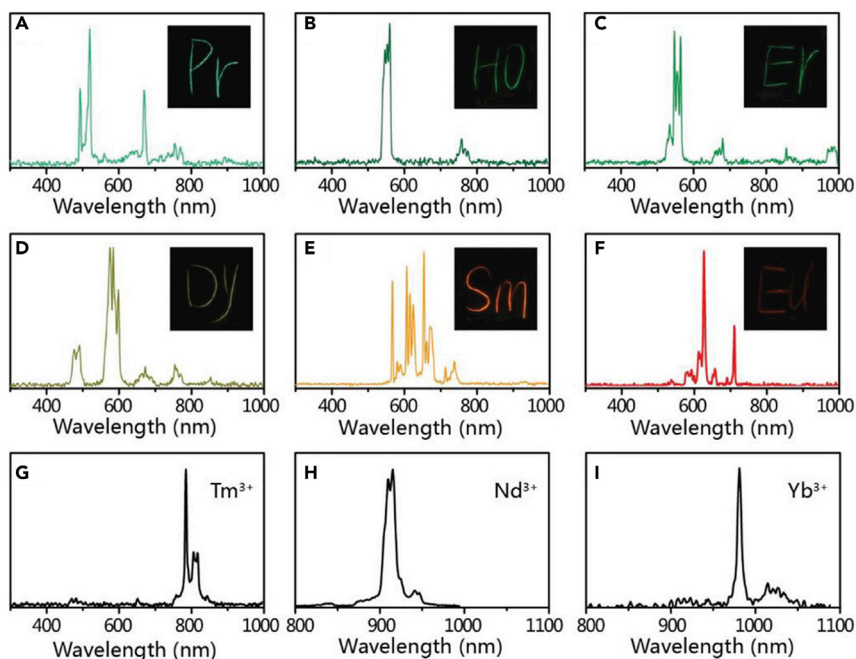
Figure 3. ML spectra of CaZnOS doped with different rare earth ions

ML spectra of CaZnOS doped with (A) Pr^{3+}, (B) Ho^{3+}, (C) Er^{3+}, (D) Dy^{3+}, (E) Sm^{3+}, (F) Eu^{3+}, (G) Tm^{3+}, (H) Nd^{3+}, and (I) Yb^{3+}. Inset: photographs of the corresponding samples under single-point dynamic pressure of a ballpoint pen. Reproduced with permission from (Du et al., 2018). Copyright 2018 WILEY.

2013). Following this idea, stable ML intensities over thousands loading cycles were obtained, but they are all limited to the visible ML range (Jeong et al., 2013; Moon Jeong et al., 2013; Wang et al., 2015; Zhou et al., 2020). One should eagerly expect that NIR ML (which can penetrate tissues) can also be self-recoverable since this will insure the *in vivo* biomechanical monitoring wherein repeated recharging by high-energy UV lights fails to work. Interestingly, in 2020, Peng et al.'s research work has reached this goal to some extent. Herein, a new class of heterojunctioned ZnS/CaZnOS piezophotonic system with remarkable ML performance in both intensity and reproducibility was demonstrated (Figure 4) (Peng et al., 2020). ZnS and CaZnOS were prepared by controlling the ratio of $CaCO_3$ and ZnS, and they accommodate Mn^{2+} and lanthanide ions (such as Tm^{3+}, Yb^{3+}, and Pr^{3+} NIR luminescent ions), respectively. Here, highly stable heterojunction was reported and was confirmed by X-ray powder diffraction, a high-resolution transmission electron microscope, and the fast Fourier transform techniques. Under a sliding force (10 N) for 20 cycles, only a marginal intensity decay was demonstrated. Notably, the ML intensity self-recovery performance here is based on the red emission of Mn^{2+}, while whether this performance is applicable to the ML in the NIR range remains to be discussed. In all, CaZnOS is one of the best NIR ML hosts, and corresponding biomechanical imaging based on this system may be possible in the near future.

$SrZn_2S_2O$ and $SrZnSO$

Indeed, one cannot deny that developing novel ML host has always been a research hotspot, which is limited to the systematical research strategies. Since MZnOS (M = Ba^{2+} or Ca^{2+} has been confirmed as one of the best ML hosts, one may easily note that another ML host can be obtained if M is replaced by Sr^{2+} cations. Following this idea, in 2019, Chen et al. developed novel MLs with super broad visible to NIR (470–1600 nm) spectra by doping lanthanide ions or transition ions into mixed anion compounds $SrZn_2S_2O$ and $SrZnSO$ (Figure 5) (Chen et al., 2020). NIR MLs were obtained both from lanthanide ions such as Tm^{3+}, Nd^{3+}, Yb^{3+}, and Er^{3+} ions in SrZnSO and Yb^{3+} ion in $SrZn_2S_2O$. Here, mixed anion compound is defined as one kind of solid-state material consisting of multiple anion species in a single phase and such were expected to be another species of ML materials. Indeed, before this work, Smet et al. have already confirmed green (~498 nm while not NIR) ML from Eu^{2+}-doped mixed anion compounds $BaSi_2O_2N_2$ and $SrSi_2O_2N_2$ (Botterman et al., 2012). However, more ML systems based on such mixed anion compounds should be exploited. As demonstrated, NIR MLs based on Er^{3+}-doped SrZnSO can be used to sense
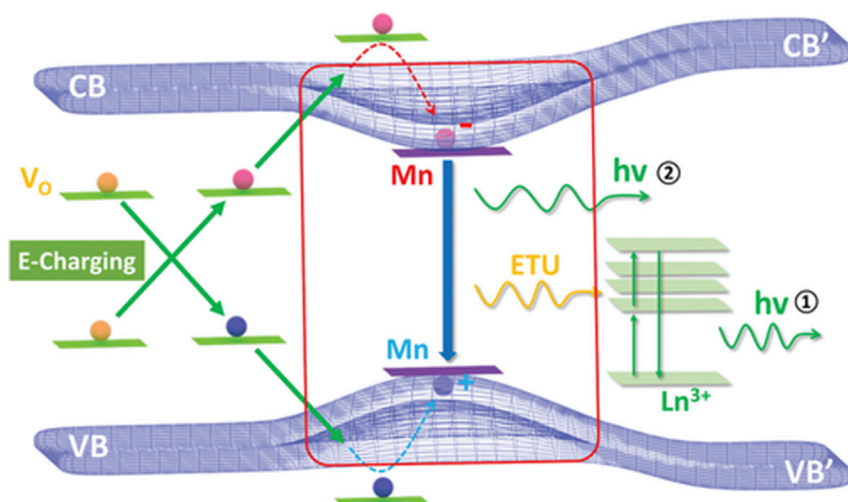
Figure 4. Scheme of proposed mechanism for mechanical-to-optical energy conversion in the piezophotonic semiconductor heterojunction

Scheme of proposed mechanism for mechanical-to-optical energy conversion in the piezophotonic semiconductor heterojunction: electronic transition in the ML process is facilitated by band offsets at the heterojunction interface region (indicated by the red frame). Reproduced with permission from (Peng et al., 2020). Copyright 2020 WILEY. VB, valence band; CB, conduction band; E-charging, electric field-induced charge separation; ETU, energy transfer upconversion; Ln^{3+}, trivalent lanthanide ion; orange balls, neutral defect centers; red balls, electrons; blue balls, holes.

bright-field stress with the help of an NIR camera. It is a promising approach for stress sensing since the least interference of ambient light (most visible lights) can be guaranteed. To address this advantage, Xiong et al. have firstly developed an NIR signature system previously (Xiong et al., 2019a). A glass rod was used to "write" on the surface of an ML pellet, and the personal abundant information (e.g. signing speed and local pressure) was recorded by NIR ML signals of an NIR camera. This work will definitely improve the anti-counterfeiting level because such NIR "signature information" cannot be read out directly by naked eyes while signing.

Oxide compounds

Aluminates

Undeniably, Eu^{2+}-doped $SrAl_2O_4$ aluminate has been one of the most famous ML systems for decades. However, it was only until 2011, Terasawa et al. declared the first NIR ML (peaked at ~1530 nm) by codoping Er^{3+} ions into $SrAl_2O_4$:Eu^{2+} (Terasawa et al., 2011). Since both Eu^{2+} or Er^{3+} singly doped $SrAl_2O_4$ failed to emit ML in the NIR range, energy transfer from Eu^{2+} to Er^{3+} ions and subsequent transition $^4I_{13/2} \rightarrow {}^4I_{15/2}$ were considered to attribute to such NIR ML emission. Unfortunately, one cannot find a clear NIR ML spectrum. In this work, only a visible light cut filter was set right in front of the photomultiplier tube to ensure that only NIR ML signals were recorded. Except for this, very recently, in 2020, Fujio et al. demonstrated that NIR ML (750–1000 nm) from Nd^{3+} was also obtained in $SrAl_2O_4$:Eu^{2+}, Cr^{3+}, and Nd^{3+}, where Eu^{2+} and Cr^{3+} ions were considered to be the sensitizer ions (Fujio et al., 2020). The NIR ML powders were synthesized by metal nitrates and malic acid, where an acid-aided method was believed to better regulate the target samples to obtain higher ML intensity. For the mechanical excitation mode, tensile testing was adopted. However, no NIR ML spectra data were also provided. On the one hand, unless by energy transfer from Eu^{2+} to Er^{3+} and Nd^{3+}, it seems "impossible" to obtain NIR MLs by singly doping in aluminate. On the other hand, one can also note NIR photoluminescence by Nd^{3+} or Er^{3+} singly doped aluminate $SrAl_2O_4$ (Ayvacıklı et al., 2013; de Herval et al., 2015). These facts indicate that NIR ML may be physically different from photoluminescence or visible ML of Eu^{2+} in $SrAl_2O_4$. The authors are eager to see more NIR MLs (at least with corresponding spectral data) in aluminates.

Gallates

(Inverse) spinel structure compound (such as $LiGa_5O_8$) has been confirmed to persistently emit after doping optically active centers such as transition metal ions (Chen et al., 2018; De Clercq et al., 2018). However, no
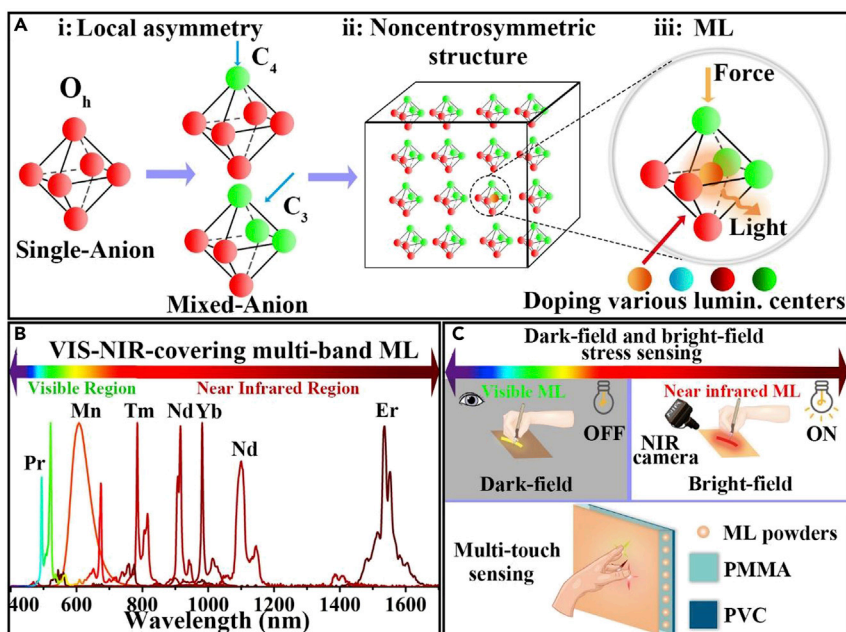
Figure 5. Design route and applications of ML materials in mixed anion compounds

(A-i) Formation of local asymmetry, e.g., C_4 or C_3 through replacing one and three ligands by other anion species. (A-ii) An overall noncentrosymmetric structure constructed by periodically aligned mixed anion polyhedrons. (A-iii) Creation of multi-color ML by doping various luminescent centers in mixed anion compounds.

(B) Multiband ML spectra covering the whole VIS-NIR region in Ln^{3+}- or Mn^{2+}-doped SrZnSO.

(C) Various applications of multi-color ML materials. The VIS ML materials can be applied to a conventional dark-field stress sensing. The NIR ML materials offer an advanced stress sensing approach operable under the natural light (bright-field sensing). Reproduced with permission from (Chen et al., 2020). Copyright 2019 Elsevier.

lanthanide ion-doped $LiGa_5O_8$ had been found to show persistent luminescence or ML until 2019. Xiong et al. realized visible to near infrared persistent luminescence by incorporation of Pr^{3+} ions into the 6 co-ordinated Li^+ sites. More interestingly, ML spectra (300–1000 nm extending into the NIR range similar to persistent luminescence) were obtained when quickly sliding a borosilicate rod on the surface of these powders (Figure 6). By normalizing the intensity of the peak at 862 nm, a comparison of peak positions and corresponding intensities between ML and persistent luminescence spectra was provided. Conclusion from this work is that mechanical rather than thermal effect plays the dominant role in the reduction of possibility of $^3P_1 \rightarrow {}^3H_J$ of Pr^{3+}. Besides, due to its persistent luminescence, one can find biological tissue penetration of the pork skin, fat, or lean in this work. Further biomechanical imaging was then expected since ML has a similar visible to NIR luminescence profile, and a larger proportion of the NIR part that can be used to penetrate tissues.

Niobates

As for niobates, in 2017, Tu et al. achieved red-emitting ML by doping Pr^{3+} ions into the piezoelectric host $LiNbO_3$ (Tu et al., 2017). It was considered the "first" piezo multifunctional material that presents both piezoelectricity and intense ML. From this work, one may find that ML signal appears once loaded, and this is indeed of great importance since a "zero threshold" ML is highly desired for practical applications. However, the underlying reason for such an efficient ML host was not fully understood at that time. For this, Huang et al. conducted a case study on alkaline niobates to deeply explain the intrinsic energy conversions for photongeneration in piezophototronic materials (Huang et al., 2018). ML mechanism was then becoming clear from the native point defect levels of $LiNbO_3$. Thanks to this work, series of ML work on niobate hosts were reported (Pan et al., 2018; Zhang et al., 2018). However, it was not until 2019 that Xiong and Peng firstly realized NIR ML (peaked at ∼895 nm) from niobate ($LiNbO_3$:Nd^{3+}) (Xiong and Peng, 2019). Under compressive load from 500 to 3000 N, NIR ML intensity increases to a maximal value at 2500 N, and further, ML intensity is limited by the mechanical strength of the resin sample. Besides, both the start and stop of the loading were confirmed to generate ML. When the load is stable, ML intensity still continuously
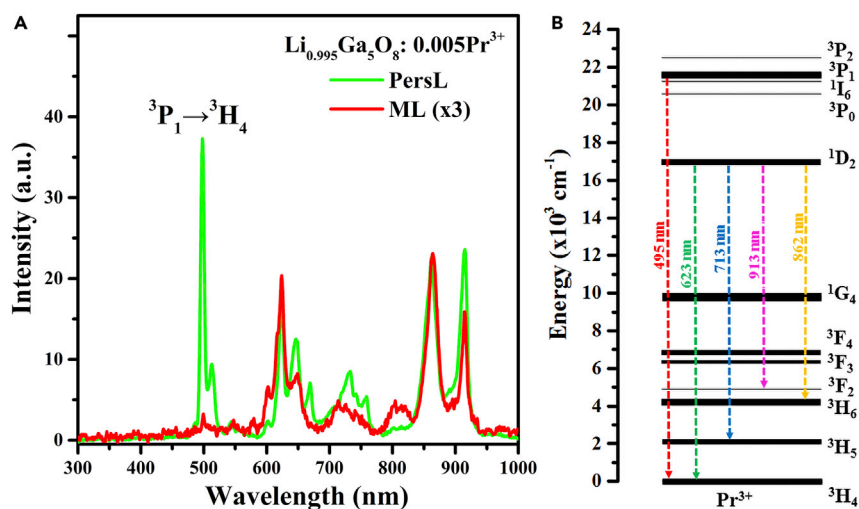
Figure 6. PersL and ML of $Li_{0.995}Ga_5O_8$:$0.005Pr^{3+}$

(A) Comparison between ML and persistent luminescence (PersL) spectra of $Li_{0.995}Ga_5O_8$:$0.005Pr^{3+}$. PersL was detected at the delay time of 2 s after pre-irradiation by a 254 nm lamp for 60 s.

(B) Energy level diagrams of Pr^{3+} ion and corresponding emission wavelengths. Reproduced with permission from (Xiong et al., 2019b). Copyright 2019 WILEY.

decreases, and finally, the stop of loading can produce only much weaker ML intensity. Importantly, ML intensity is highly trap dependent, such as shallow traps may result in lower ML intensity; for more details, one can refer to previous work on $BaSi_2O_2N_2$ (Botterman et al., 2012). Finally, as a proof of concept of bio-penetration, tissues such as the pork skin, fat, and meat were used, and the best penetration depth reaches 22 mm (Figure 7). Hence, *in situ*, real-time, and *in vivo* biomechanical sensing was further expected to realize. Also, since stable load generates no ML, we also believe that only pulsed biomechanical behaviors can be visualized using ML techniques. For this, one can find more evidence in the heartbeat-sensing ML device (Wang et al., 2020).

Stannates

Regarding the possible ML hosts, layered Ruddlesden-Popper perovskite such as stannates $Sr_{n+1}Sn_nO_{3n+1}$ (n = 1, 2, ..., ∞) should be one of the best efficient ML hosts. Temperature switchable polarization of bulk crystals has been confirmed, and such nature is closely related to piezoelectricity that desired for ML (Oh et al., 2015). Generally, ML performances of such layered structure materials are strongly dependent on the number of the layers. For example, Sm^{3+}-doped $Sr_3Sn_2O_7$ has the best ML intensity compared to that of Sr_2SnO_4 and $SrSnO_3$ (Kamimura et al., 2012). The ML performances also can be largely improved such as by tailoring the band gap and trap distribution (Li et al., 2018a). However, only visible MLs were reported before. Afterward, by incorporating Nd^{3+} ions into $Sr_3Sn_2O_7$, Xiong et al. confirmed its NIR ML emission in 2019 (Xiong et al., 2019a). Under compressive load or friction, same NIR ML spectra (peaked at ~900 nm) located within the first biowindow were observed. Moreover, such emission is recoverable as ML intensity can be fully restored if recharged by high-energy 254-nm light irradiation. Except for NIR ML centers of Nd^{3+} ions, it was particularly meaningful that NIR ML from intrinsic defects (700–850 nm) was observed. And such intrinsic NIR MLs should be enhanced by doping Nd^{3+} ions because nearly no such signals appear from the blank sample. Namely, the incorporation of Nd^{3+} has bridged the energy transfer from external force to $Sr_3Sn_2O_7$. Results from thermoluminescence indicated an easy way to selectively quench the NIR ML of the host by just prolonging the detection time. Finally, to demonstrate its biomechanical bioimaging possibility, pigskin and hydroxyl apatite (HAP, which is the main component of human bones) were chosen to simulate "muscles" and "bones", respectively. Interestingly, such NIR ML emissions can penetrate both of them, and the deepest penetration depth for pigskin reaches ~30 mm (Figure 8). These facts may have provided a possible way to realize *in situ* biomechanical behavior visualization.

After this work, in 2020, Tu et al. also reported NIR ML emissions from Nd^{3+}-doped $Sr_3Sn_2O_7$ (Tu et al., 2020). Totally, $Sr_3Sn_2O_7$ reported from both researchers belong to the same orthorhombic crystal
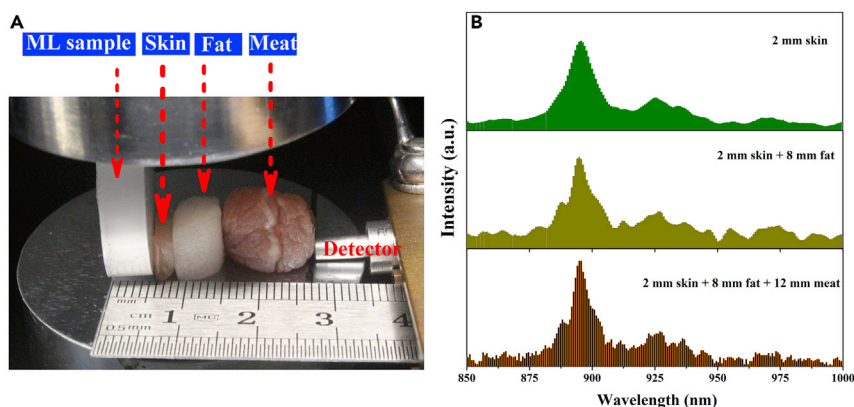
Figure 7. Biological tissue penetration experiments

(A and B) (A) The thickest tissue used in this test; (B) ML spectra under 1000 N after passing through different tissue samples: (top) 2 mm skin; (middle) 2 mm skin +8 mm fat; and (bottom) 2 mm skin +8 mm fat +12 mm meat. Reproduced with permission from (Xiong and Peng, 2019). Copyright 2019 Royal Society of Chemistry.

system, while the space groups are reported to be $A2_1am$ by Tu et al. and $Cmcm$ by Xiong et al. Such differences made $Sr_3Sn_2O_7:Nd^{3+}$ ($A2_1am$) a "true" elastic deformation-induced ML with improved sustainability and ultrasensitivity. Namely, 800–1500 nm NIR MLs were induced at micro-strain levels, which are enhanced by the ferroelectrically polarized charges in $Sr_3Sn_2O_7$ ($A2_1am$). Notably, as a proof of biomechanical imaging, fresh chicken skin and pork ($\sim$5 mm in thickness) were used to cover the surface of ML pellets, and the obtained NIR ML intensity was believed sufficient for biomechanical imaging of implanted materials within small animals. NIR ML signals were recorded *in situ* using an InGaAs CCD camera with a spectral sensitivity between 900 and 1700 nm (Figure 9). It is worth emphasizing that such NIR ML crystals will accelerate the application for bioscience *in situ* under both light and dark conditions.

CONCLUSIONS AND OUTLOOK

Although ML crystals (used as mechanical sensor probes) have be widely known around our daily life for a long time, their use as mechanical sensor probes was only refocused on until $\sim$1999. The elastic ML intensities of ZnS:Mn and $SrAl_2O_4:Eu^{2+}$ linearly correspond to external mechanical stimuli while keeping complete crystal structure and advanced this field to a big step since then. Notably, lots of ML crystals have been found and corresponding potential applications have been demonstrated. However, their use in bioimaging has achieved limited progress, which is mostly limited to the number of such NIR ML crystals. One can easily note that no more than 11 ML crystals can emit NIR emissions (Table 1). Then, a detailed review of these crystals has been provided, concerning the crystal system, space group, and chemical environments. It is suggested that NIR ML crystals should better be non-centrosymmetric as hexagonal, orthorhombic, monoclinic, or cubic. High piezoelectric oxysulfide semiconductor such as CaZnOS still dominates the number of NIR ML hosts. Besides, not all NIR optical centers can be used as NIR ML dopants, and Nd^{3+} ion should always have been the best choice. To demonstrate the tissue penetrating ability of those NIR ML crystals *in vitro*, soft tissue pork is always chosen, as well as chicken sometimes. Sclerous tissues such as human teeth and HAP have also been confirmed not to prevent from penetration by those NIR ML emissions. Besides, no *in vivo* bioimaging has been provided and this should be of importance in next step development. Except for those, other outlooks also should be addressed, and further directions may include the following:

(1) Gaining more insights into the behind NIR ML mechanism

Even today, controversies over the mechanism of ML remain, let alone that of NIR ML. For example, ML mechanism of $SrAl_2O_4:Eu$ and ZnS:Mn mostly consisted of such processes: detrapping carriers at shallow traps under mechanical stimuli and, afterward, activator recombination occurs with the local piezoelectric field. However, Sohn et al. insisted on that the triboelectricity-induced luminescence works in ZnS:Cu-polydimethylsiloxane composite due to its poor piezoelectric properties (Sohn et al., 2016).
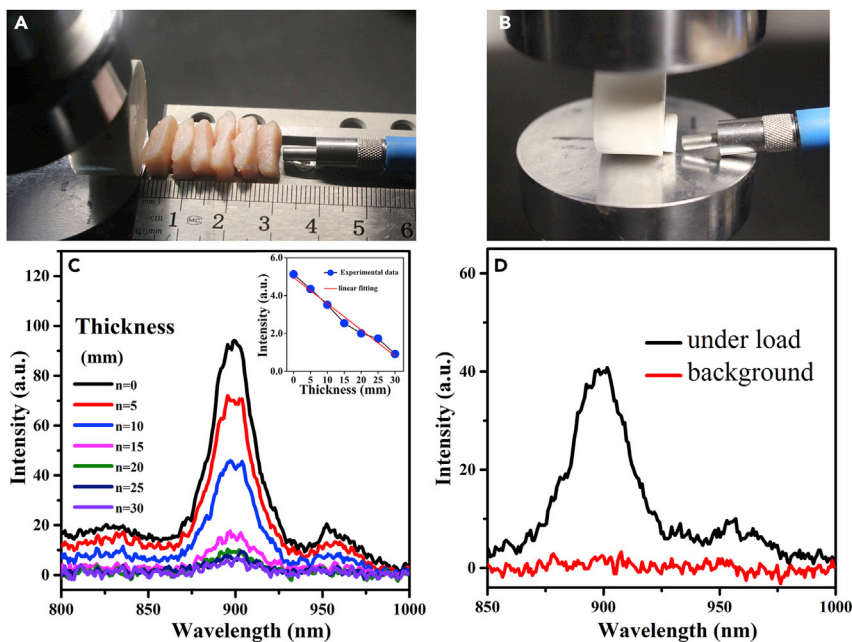
Figure 8. Tissue penetration experiments

(A) and (B) are the experimental detection images of penetrating pigskin and HAP, respectively.

(C) ML spectra after passing through different thicknesses of pigskins, which increases 5 mm each time from 0 to 30 mm. The inset is the integrated ML intensities over the spectral range of 870–970 nm of these spectra shown in (C).

(D) ML spectra passing through HAP pellet and the background signal. Reproduced with permission from (Xiong et al., 2019a). Copyright 2019 The American Ceramic Society.

Generally, most ML materials can be excited by friction, while not all of them can easily emit under compression (e. g. $LiGa_5O_8$: Pr^{3+}). Nowadays, researchers tend to simply attribute them to a so-called piezoelectric field-induced trap detrapping model, while no corresponding piezoelectric parameters have been provided. Hence, it is suggested that researchers pay more attention to their statements in explaining ML mechanisms. Besides, does NIR ML really share the same ML mechanism with that of visible ML?

(2) Establishing the possible relation between the possibilities of generating ML and its emission centers

One can easily note that Eu^{2+} dominates the number of visible MLs, while Nd^{3+} accounts for the vast majority of NIR MLs (Figure 1 and Table 1). So, one may propose that are Eu^{2+} and Nd^{3+} more sensitive to external mechanical stimuli than other ions? Hence, can ML be the intrinsic properties of these luminescent ions and their response to mechanical stimuli is intrinsically inclined? In a word, researchers who are good at luminescence should participate in this field to help solve this problem.

(3) Exploring more practical applications for NIR ML

Remarkably, NIR ML can penetrate tissues and realize in situ, real-time, and non-destructive visualization of internal biostress. One can expect that such technique is promising for monitoring the mechanical strength of an implanted component. However, although several NIR ML crystals have been confirmed, the tissue penetrations have only been demonstrated in vitro (e.g. $Sr_3Sn_2O_7$:Nd [Tu et al., 2020; Xiong et al., 2019a], $LiNbO_3$:Nd [Xiong and Peng, 2019], and CaZnOS:Nd [Li et al., 2018b]). Regarding the use in vivo, it is suggested that those NIR ML crystals should be smaller in size and having them nanosized (which is usually more biocompatible) is thus worth expecting. Besides, except for biomechanical sensor of NIR ML, other applications such as dynamic pressure mapping (Xiong et al., 2019a) and bright-field stress visualization (Chen et al., 2020) should be focused on since such NIR ML signals cannot be observed directly by naked eyes.
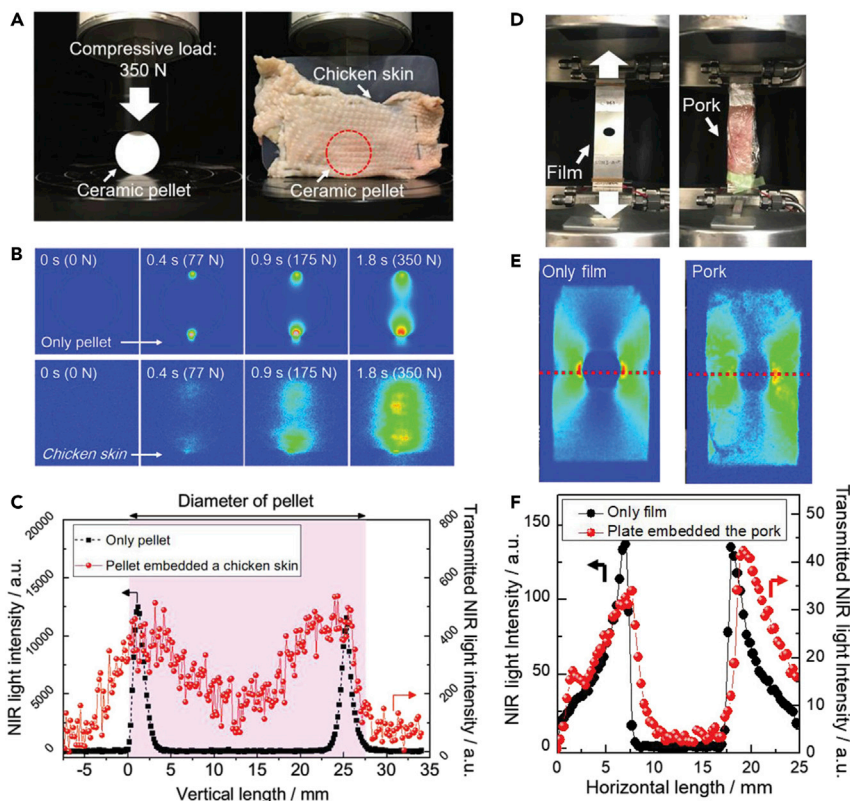
Figure 9. Tissue penetration experiments for SSN
(A) CCD images for SSN (Sr$_3$Sn$_2$O$_7$:Nd^{3+}) pellet set.
(B) Sequence of images recorded using an InGaAs-CCD camera for SSN applied during the load cycle of 350 N at a rate of 3 mm min-1 showing the real-time images of NIR light distribution.
(C) The distribution along vertical component of the NIR piezoluminescence in the SSN pellet with and without a chicken skin under a compressive load of 77 N.
(D) CCD image for Sr$_3$Sn$_2$O$_7$:Nd^{3+} (SSN) flm.
(E) Images recorded with an InGaAs-CCD camera for SSN flm by tensile load applied (nominal strain: 600 μst).
(F) The distribution at the horizontal position along the center of a circular hole of the NIR piezoluminescence of the SSN flm outside and embedded 5 mm in a sample of pork under a tensile load (maximum of nominal strain: 600 μst).
Reproduced with permission from (Tu et al., 2020). Copyright 2020 WILEY.

(4) Developing diversified NIR ML centers. Notably, most known NIR ML centers are from lanthanide ions

Exceptionally, Xiong et al. once attributed the NIR ML within 700–850 nm of Sr$_3$Sn$_2$O$_7$:Nd^{3+} to the host, which was confirmed since similar photoluminescence was observed. Although no clear evidence has been provided, this finding has certain guiding significance for widening existed understanding of the nature of NIR ML centers.

(5) Organisms have complex biomechanical behaviors, and these biostresses are varied in tissues

Thus, it is of importance to evaluate the required pressure levels of mechanical stimuli for bioimaging such as in vivo, in vitro, electronic skins, prosthetics, false tooth, etc. For this, professional medical researchers are suggested to be invited in. From another perspective, it is quite important to develop NIR ML materials with ultra-low or even zero threshold. This low threshold NIR ML crystal may come from ML material itself such as high piezoelectric system of LiNbO$_3$:Pr^{3+}, whose "zero" ML threshold has been reported, since immediate ML signal can be observed once load appears (Tu et al., 2017) or else designing modification architecture to enhance the sensitivity of ML devices. Following this idea, a skin-driven ML (namely, ML induced by the movement by lips corner, canthus, and cheek) has been demonstrated (Qian et al., 2018). Both strategies should be focused on in developing ultra-low/even zero threshold NIR MLs.

Finally, we want to encourage researchers to think ML with physics. If force causes deformation and produces light and this effect is reciprocal, that is, using light to achieve stress deformation, even this deformation may be small. Then, if you can measure this tiny deformation, you may reveal its physical ML mechanism. How to realize the measurement of such tiny deformations still needs light realization. Researchers who focus on ultrafast lasers, especially those who do Brillouin nonlinear effects, may provide professional suggestions. In all, NIR ML is expected to bring out other promising applications due to the combination of ML and NIR spectral techniques. It will open path toward the realization of encouraging applications *in vivo* bioimaging and fundamental research.

AUTHOR CONTRIBUTIONS

Conceptualization: P.X.X and M.Y.P, Writing-original draft: P.X.X, Visualization: M.Y.P, Supervision: M.Y.P. Revision: P.X.X and Z.M.Y.

DECLARATION OF INTERESTS

The authors believe that there is no interest to declare.

REFERENCES

Afsarimanesh, N., Mukhopadhyay, S.C., and Kruger, M. (2018). Sensing technologies for monitoring of bone-health: a review. Sens. Actuators A *274*, 165–178.

Akiyama, M., Xu, C.-n., Nonaka, K., and Watanabe, T. (1998). Intense visible light emission from $Sr_3Al_2O_6$:Eu,Dy. Appl. Phys. Lett. *73*, 3046–3048.

Ayvacıklı, M., Kotan, Z., Ekdal, E., Karabulut, Y., Canimoglu, A., Garcia Guinea, J., Khatab, A., Henini, M., and Can, N. (2013). Solid state synthesis of $SrAl_2O_4$:Mn^{2+} co-doped with Nd^{3+} phosphor and its optical properties. J. Lumin. *144*, 128–132.

Bacon, F. (1863). The two books of Francis Bacon: of the proficience and advancement of learning. In The two books of Francis Bacon: of the proficience and advancement of learning, T. Markby, ed. (Parker, Son, and Bourn).

Bao, L., Xu, X., Zuo, Y., Zhang, J., Liu, F., Yang, Y., Xu, F., Sun, X., and Peng, H. (2019). Piezoluminescent devices by designing array structures. Sci. Bull. *64*, 151–157.

Botterman, J., Eeckhout, K.V.d., Baere, I.D., Poelman, D., and Smet, P.F. (2012). Mechanoluminescence in $BaSi_2O_2N_2$:Eu. Acta Mater. *60*, 5494–5500.

Chandra, V.K., Chandra, B.P., and Jha, P. (2013). Self-recovery of mechanoluminescence in ZnS:Cu and ZnS:Mn phosphors by trapping of drifting charge carriers. Appl. Phys. Lett. *103*, 161113.

Chen, C., Zhuang, Y., Tu, D., Wang, X., Pan, C., and Xie, R.-J. (2020). Creating visible-to-near-infrared mechanoluminescence in mixed-anion compounds $SrZn_2S_2O$ and SrZnSO. Nano Energy *68*, 104329.

Chen, Y.F., Liu, F., Liang, Y.J., Wang, X.L., Bi, J.Q., Wang, X.J., and Pan, Z.W. (2018). A new up-conversion charging concept for effectively charging persistent phosphors using low-energy visible-light laser diodes. J. Mater. Chem. C *6*, 8003–8010.

Clays, K., and Persoons, A. (1991). Hyper-Rayleigh scattering in solution. Phys. Rev. Lett. *66*, 2980–2983.

De Clercq, O.Q., Du, J., Smet, P.F., Joos, J.J., and Poelman, D. (2018). Predicting the afterglow duration in persistent phosphors: a validated approach to derive trap depth distributions. Phys. Chem. Chem. Phys. *20*, 30455–30465.

de Herval, L.K.S., Tuncer Arslanlar, Y., Ayvacikli, M., Iikawa, F., Nobrega, J.A., Pizani, P.S., Galvão Gobato, Y., Can, N., Henini, M., and de Godoy, M.P.F. (2015). Enhancement of the luminescence intensity by co-doping Mn^{2+} into Er^{3+}-doped $SrAl_2O_4$. J. Lumin. *163*, 17–20.

Du, Y., Jiang, Y., Sun, T., Zhao, J., Huang, B., Peng, D., and Wang, F. (2018). Mechanically excited multicolor luminescence in lanthanide ions. Adv. Mater. *31*, e1807062.

Eddingsaas, N.C., and Suslick, K.S. (2006). Mechanoluminescence: light from sonication of crystal slurries. Nature *444*, 163.

Feng, A., and Smet, A.P.F. (2018). A review of mechanoluminescence in inorganic solids: compounds, mechanisms, models and applications. Materials (Basel) *11*, 484.

Fujio, Y., Xu, C.-N., and Terasaki, N. (2020). Synthesis of near-infrared mechanoluminescence material via organic acid-aided process. ECS Trans. *98*, 61–68.

Hardy, G., Chandra, B., Zink, J.I., Adamson, A.W., Fukuda, R.C., and Walters, R.T. (1979). Pulsed infrared laser induced visible luminescence. J. Am. Chem. Soc. *101*, 2787–2788.

Huang, B., Peng, D., and Pan, C. (2017a). "Energy Relay Center" for doped mechanoluminescence materials: a case study on Cu-doped and Mn-doped CaZnOS. Phys. Chem. Chem. Phys. *19*, 1190–1208.

Huang, B., Sun, M., and Peng, D. (2018). Intrinsic energy conversions for photon-generation in piezo-phototronic materials: a case study on alkaline niobates. Nano Energy *47*, 150–171.

Huang, L., Zhou, Y., Meng, L., Wu, D., and He, Y. (2017b). Comparison of different CCD detectors and chemometrics for predicting total anthocyanin content and antioxidant activity of mulberry fruit using visible and near infrared hyperspectral imaging technique. Food Chem. *224*, 1–10.

Incel, A., Emirdag-Eanes, M., McMillen, C.D., and Demir, M.M. (2017). Integration of triboluminescent EuD4TEA crystals to transparent polymers: impact sensor application. ACS Appl. Mater. Interfaces *9*, 6488–6496.

Jeong, S.M., Song, S., Joo, K.-I., Kim, J., Hwang, S.-H., Jeong, J., and Kim, H. (2014). Bright, wind-driven white mechanoluminescence from zinc sulphide microparticles embedded in a polydimethylsiloxane elastomer. Energy. Environ. Sci. *7*, 3338–3346.

Jeong, S.M., Song, S., Lee, S.K., and Ha, N.Y. (2013). Color manipulation of mechanoluminescence from stress-activated composite films. Adv. Mater. *25*, 6194–6200.

CellPress
OPEN ACCESS

Kamimura, S., Yamada, H., and Xu, C.-N. (2012). Strong reddish-orange light emission from stress-activated $Sr_{n+1}Sn_nO_{3n+1}$:Sm^{3+} (n = 1, 2, ∞) with perovskite-related structures. Appl. Phys. Lett. *101*, 091113.

Kundu, T., Terasaki, N., Xu, C.-N., Li, C., Zhang, L., Li, C., Ono, D., Tsubai, M., Adachi, Y., Imai, Y., et al. (2012). Visualization of active crack on bridge in use by mechanoluminescent sensor. Inter. Soc. Opt. Photo. *8348*, 83482D.

Larson, C., Peele, B., Li, S., Robinson, S., Totaro, M., Beccai, L., Mazzolai, B., and Shepherd, R. (2016). Highly stretchable electroluminescent skin for optical signaling and tactile sensing. Science *351*, 1071–1074.

Li, J., Xu, C.-N., Tu, D., Chai, X., Wang, X., Liu, L., and Kawasaki, E. (2018a). Tailoring bandgap and trap distribution via Si or Ge substitution for Sn to improve mechanoluminescence in $Sr_3Sn_2O_7$:Sm^{3+} layered perovskite oxide. Acta Mater. *145*, 462–469.

Li, L., Wondraczek, L., Li, L., Zhang, Y., Zhu, Y., Peng, M., and Mao, C. (2018b). CaZnOS:Nd^{3+} emits tissue-penetrating near-infrared light upon force loading. ACS Appl. Mater. Interfaces *10*, 14509–14516.

Li, L., Wondraczek, L., Peng, M., Ma, Z., and Zou, B. (2020). Force-induced 1540 nm luminescence: role of piezotronic effect in energy transfer process for mechanoluminescence. Nano Energy *69*, 104413.

Li, W., Huang, Q., Mao, Z., Li, Q., Jiang, L., Xie, Z., Xu, R., Yang, Z., Zhao, J., Yu, T., et al. (2018c). Alkyl chain introduction: in-situ solar-renewable organic colorful mechanoluminescence materials. Angew. Chem. Int. Ed. *57*, 12727–12732.

Liu, L., and Webster, T.J. (2016). In situ sensor advancements for osteoporosis prevention, diagnosis, and treatment. Curr. Osteoporos. Rep. *14*, 386–395.

Matsui, H., Xu, C.-N., Akiyama, M., and Watanabe, T. (2000). Strong mechanoluminescence from UV-irradiated spinels of $ZnGa_2O_4$: Mn and $MgGa_2O_4$: Mn. Jp. J. Appl. Phys. *39*, 6582.

Moon Jeong, S., Song, S., Lee, S.-K., and Choi, B. (2013). Mechanically driven light-generator with high durability. Appl. Phys. Lett. *102*, 051110.

Oh, Y.S., Luo, X., Huang, F.-T., Wang, Y., and Cheong, S.-W. (2015). Experimental demonstration of hybrid improper ferroelectricity and the presence of abundant charged walls in $(Ca,Sr)_3Ti_2O_7$ crystals. Nat. Mater. *14*, 407–413.

Pan, C., Zhang, J.-C., Zhang, M., Yan, X., Zhang, H.-D., Long, Y.-Z., Sun, X.-Y., and Jiang, H.-T. (2018). Trap-controlled mechanoluminescence in Pr3+-activated M2Nb2O7 (M = Sr, Ca) isomorphic perovskites. Opt. Mater. Express *8*, 1425.

Park, H.J., Kim, S., Lee, J.H., Kim, H.T., Seung, W., Son, Y., Kim, T.Y., Khan, U., Park, N.M., and Kim, S.W. (2019). Self-powered motion-driven triboelectric electroluminescence textile system. ACS Appl. Mater. Interfaces *11*, 5200–5207.

Peng, D., Jiang, Y., Huang, B., Du, Y., Zhao, J., Zhang, X., Ma, R., Golovynskyi, S., Chen, B., and Wang, F. (2020). A ZnS/CaZnOS heterojunction for efficient mechanical-to-optical energy conversion by conduction band offset. Adv. Mater. *32*, 1907747.

Qian, X., Cai, Z., Su, M., Li, F., Fang, W., Li, Y., Zhou, X., Li, Q., Feng, X., Li, W., et al. (2018). Printable skin-driven mechanoluminescence devices via nanodoped matrix modification. Adv. Mater. *30*, 1800291.

Sohn, K.-S., Timilsina, S., Singh, S.P., Choi, T., and Kim, J.S. (2016). Mechanically driven luminescence in a ZnS:Cu-PDMS composite. APL Mater. *4*, 106102.

Tan, Y.J., Godaba, H., Chen, G., Tan, S.T.M., Wan, G., Li, G., Lee, P.M., Cai, Y., Li, S., Shepherd, R.F., et al. (2020). A transparent, self-healing and high-κ dielectric for low-field-emission stretchable optoelectronics. Nat. Mater. *19*, 182–188.

Terasaki, N., Yamada, H., and Xu, C.-N. (2013). Ultrasonic wave induced mechanoluminescence and its application for photocatalysis as ubiquitous light source. Catal. Today *201*, 203–208.

Terasawa, Y., Xu, C., Yamada, H., and Kubo, M. (2011). Near infra-red mechanoluminescence from strontium aluminate doped with rare-earth ions. IOP Conf. Ser.: Mater. Sci. Eng. *18*, 212013.

Tu, D., Xu, C.-N., and Fujio, Y. (2014). Intense red emitting mechanoluminescence from CaZnOS:Mn,Li with c-axis preferred orientation. J. Adv. Dielec. *04*, 1450017.

Tu, D., Xu, C.-N., Fujio, Y., and Yoshida, A. (2015). Tuning the mechano-optical conversion in CaZnOS with Cu ion concentration. J. Phys. D: Appl. Phys. *48*, 475105.

Tu, D., Xu, C.N., Kamimura, S., Horibe, Y., Oshiro, H., Zhang, L., Ishii, Y., Hyodo, K., Marriott, G., Ueno, N., et al. (2020). Ferroelectric $Sr_3Sn_2O_7$:Nd^{3+}: a new multipiezo material with ultrasensitive and sustainable near-infrared piezoluminescence. Adv. Mater. *32*, 1908083.

Tu, D., Xu, C.N., Yoshida, A., Fujihala, M., Hirotsu, J., and Zheng, X.G. (2017). LiNbO3:Pr^{3+} : a multipiezo material with simultaneous piezoelectricity and sensitive piezoluminescence. Adv. Mater. *29*, 1606914.

Wang, C., Yu, Y., Yuan, Y., Ren, C., Liao, Q., Wang, J., Chai, Z., Li, Q., and Li, Z. (2020). Heartbeat-sensing mechanoluminescent device based on a quantitative relationship between pressure and emissive intensity. Matter *2*, 181–193.

Wang, W., Peng, D., Zhang, H., Yang, X., and Pan, C. (2017). Mechanically induced strong red emission in samarium ions doped piezoelectric semiconductor CaZnOS for dynamic pressure sensing and imaging. Opt. Commun. *395*, 24–28.

Wang, X., Peng, D., Huang, B., Pan, C., and Wang, Z.L. (2019). Piezophotonic effect based on mechanoluminescent materials for advanced flexible optoelectronic applications. Nano Energy *55*, 389–400.

Wang, X., Xu, C.N., Yamada, H., Nishikubo, K., and Zheng, X.G. (2005). Electro-mechano-optical conversions in Pr^{3+}-doped $BaTiO_3$–$CaTiO_3$ ceramics. Adv. Mater. *17*, 1254–1258.

Wang, X., Zhang, H., Yu, R., Dong, L., Peng, D., Zhang, A., Zhang, Y., Liu, H., Pan, C., and Wang, Z.L. (2015). Dynamic pressure mapping of personalized handwriting by a flexible sensor matrix based on the mechanoluminescence process. Adv. Mater. *27*, 2324–2331.

Wu, C., Zeng, S., Wang, Z., Wang, F., Zhou, H., Zhang, J., Ci, Z., and Sun, L. (2018). Efficient mechanoluminescent elastomers for dual-responsive anticounterfeiting device with stretching/strain sensor with multimode sensibility. Adv. Funct. Mater. *28*, 1803168.

Wu, X., Zhu, X., Chong, P., Liu, J., Andre, L.N., Ong, K.S., Brinson, K., Jr., Mahdi, A.I., Li, J., Fenno, L.E., et al. (2019). Sono-optogenetics facilitated by a circulation-delivered rechargeable light source for minimally invasive optogenetics. Proc. Natl. Acad. Sci. U S A *116*, 26332–26342.

Xie, Y., and Li, Z. (2018). Triboluminescence: recalling interest and new aspects. Chem *4*, 943–971.

Xiong, P., and Peng, M. (2019). Near infrared mechanoluminescence from the Nd^{3+} doped perovskite LiNbO3:Nd^{3+} for stress sensors. J. Mater. Chem. C *7*, 6301–6307.

Xiong, P., Peng, M., Cao, J., and Li, X. (2019a). Near infrared mechanoluminescence from $Sr_3Sn_2O_7$: Nd^{3+} for in situ biomechanical sensor and dynamic pressure mapping. J. Amer. Cera. Soc. *102*, 5899–5909.

Xiong, P., Peng, M., Qin, K., Xu, F., and Xu, X. (2019b). Visible to near-infrared persistent luminescence and mechanoluminescence from Pr^{3+}-doped $LiGa_5O_8$ for energy storage and bioimaging. Adv. Opt. Mater. *7*, 1901107.

Xu, C.-N., Watanabe, T., Akiyama, M., and Zheng, X.-G. (1999a). Direct view of stress distribution in solid by mechanoluminescence. Appl. Phys. Lett. *74*, 2414–2416.

Xu, C.N., Watanabe, T., Akiyama, M., and Zheng, X.G. (1999b). Artificial skin to sense mechanical stress by visible light emission. Appl. Phys. Lett. *74*, 1236–1238.

Xu, C.-N., Zheng, X.-G., Akiyama, M., Nonaka, K., and Watanabe, T. (2000). Dynamic visualization of stress distribution by mechanoluminescence image. Appl. Phys. Lett. *76*, 179–181.

Zhang, H., Peng, D., Wang, W., Dong, L., and Pan, C. (2015). Mechanically induced light emission and infrared-laser-induced upconversion in the Er-doped CaZnOS multifunctional piezoelectric semiconductor for optical pressure and temperature sensing. J. Phys. Chem. C *119*, 28136–28142.

Zhang, J.-C., Wang, X., Marriott, G., and Xu, C.-N. (2019). Trap-controlled mechanoluminescent materials. Pro. Mater. Sci. *103*, 678–742.

Zhang, J.-C., Xu, C.-N., Kamimura, S., Terasawa, Y., Yamada, H., and Wang, X. (2013). An intense elastico-mechanoluminescence material CaZnOS:Mn^{2+} for sensing and imaging multiple mechanical stresses. Opt. Express *21*, 12976.

Zhang, J.C., Pan, C., Zhu, Y.F., Zhao, L.Z., He, H.W., Liu, X., and Qiu, J. (2018). Achieving thermo-mechano-opto-responsive bitemporal colorful luminescence via multiplexing of dual lanthanides in piezoelectric particles and its multidimensional anticounterfeiting. Adv. Mater. *30*, e1804644.

Zhang, L., Xu, C.-N., Yamada, H., and Bu, N. (2010). Enhancement of mechanoluminescence in $CaAl_2Si_2O_8:Eu^{2+}$ by partial Sr^{2+} substitution for Ca^{2+}. J. Electro. Soc. *157*, J50.

Zhang, X., Zhao, J., Chen, B., Sun, T., Ma, R., Wang, Y., Zhu, H., Peng, D., and Wang, F. (2020a). Tuning multimode luminescence in lanthanide(III) and manganese(II) Co-doped CaZnOS crystals. Adv. Opt. Mater. *8*, 2000274.

Zhang, Y., Zhang, X., Wang, H., Tian, Y., Pan, H., Zhang, L., Wang, F., and Chang, J. (2020b). Remote regulation of optogenetic proteins by a magneto-luminescence microdevice. Adv. Funct. Mater. 2006357, https://doi.org/10.1002/adfm. 202006357.

Zhou, J., Gu, Y., Lu, J., Xu, L., Zhang, J., Wang, D., and Wang, W. (2020). An ultra-strong non-pre-irradiation and self-recoverable mechanoluminescent elastomer. Chem. Engin. J. *390*, 124473.

Zhuang, Y., Tu, D., Chen, C., Wang, L., Zhang, H., Xue, H., Yuan, C., Chen, G., Pan, C., Dai, L., et al. (2020). Force-induced charge carrier storage: a new route for stress recording. Light. Sci. Appl. *9*, 182.